European Radiology (2019) 29:5403–5414
https://doi.org/10.1007/s00330-019-06088-w

ONCOLOGY

IVIM improves preoperative assessment of microvascular invasion in HCC

Yi Wei[1] · Zixing Huang[1] · Hehan Tang[1] · Liping Deng[1] · Yuan Yuan[1] · Jiaxing Li[2] · Dongbo Wu[3] · Xiaocheng Wei[4] · Bin Song[1]

Received: 18 September 2018 / Revised: 2 February 2019 / Accepted: 8 February 2019 / Published online: 15 March 2019

Abstract

Purpose To prospectively evaluate the potential role of intravoxel incoherent motion (IVIM) and conventional radiologic features for preoperative prediction of microvascular invasion (MVI) in patients with hepatocellular carcinoma (HCC).

Methods Institutional review board approval and written informed consent were obtained for this study. A cohort comprising 115 patients with 135 newly diagnosed HCCs between January 2016 and April 2017 were evaluated. Two radiologists independently reviewed the radiologic features and the apparent diffusion coefficient (ADC), true diffusion coefficient (*D*), pseudodiffusion coefficient (*D**), and pseudodiffusion component fraction (*f*) were also measured. Interobserver agreement was checked and univariate and multivariate logistic regressions were used for screening the risk factors. Receiver operating characteristics (ROC) curve analyses were performed to evaluate the diagnostic performance.

Results Features significantly related to MVI of HCC at univariate analysis were reduced ADC (odds ratio, 0.341; 95% CI, 0.211–0.552; $p < 0.001$), *D* (odds ratio, 0.141; 95% CI, 0.067–0.299; $p < 0.001$), and irregular circumferential enhancement (odds ratio, 9.908; 95% CI, 3.776–25.996; $p < 0.001$). At multivariate analysis, only *D* value (odds ratio, 0.096; 95% CI, 0.025–0.364; $p < 0.001$) was the independent risk factor for MVI of HCC. The mean *D* value for MVI of HCC showed an area under ROC curves of 0.815 (95% CI, 0.740–0.877).

Conclusion IVIM model–derived *D* value is superior to ADC measured with mono-exponential model for evaluating the MVI of HCC. Among MR imaging features, tumor margin, enhancement pattern, tumor capsule, and peritumoral enhancement were not predictive for MVI.

Key Points

- *Diffusion MRI is useful for non-invasively evaluating the microvascular invasion of hepatocellular carcinoma.*
- *IVIM model is advantageous over mono-exponential model for assessing the microvascular invasion of hepatocellular carcinoma.*
- *Decreased D value was the independent risk factor for predicting MVI of HCC.*

Keywords Magnetic resonance imaging · Hepatocellular carcinoma · Diagnostic imaging

Yi Wei and Zixing Huang contributed equally to this work.

✉ Bin Song
songlab_radiology@163.com

[1] Department of Radiology, West China Hospital, Sichuan University, Chengdu 610041, China

[2] Department of Liver Surgery, West China Hospital, Sichuan University, Chengdu, China

[3] Center of Infectious Diseases, West China Hospital, Sichuan University, Chengdu, China

[4] GE Healthcare China, Beijing, China

Abbreviations

^{18}F-FDG	^{18}F-fluorodeoxyglucose
ADC	Apparent diffusion coefficient
AUC	Area under curve
CI	Confidence interval
CT	Computed tomography
D	True diffusion coefficient
*D**	Pseudodiffusion coefficient
DWI	Diffusion-weighted imaging
f	Pseudodiffusion component fraction
HCC	Hepatocellular carcinoma
ICC	Intra-class correlation coefficient

IVIM	Intravoxel incoherent motion
LAVA	Liver acceleration volume acquisition
MRI	Magnetic resonance imaging
MVI	Microvascular invasion
OR	Odds ratio
PET	Positron emission tomography
ROC	Receiver operating characteristics
ROI	Region of interest
WTV	Whole tumor volume

Introduction

Hepatocellular carcinoma (HCC) is the fifth most common cancer worldwide, and the second leading cause of cancer-related deaths [1]. Hepatic resection, transplantation, and percutaneous ablation have been regarded as the most effective treatment of HCC, and hepatectomy is considered as the best approach for patients with well-preserved liver function [2, 3]. High postoperative recurrence, however, still leads to a poor prognosis of HCC [4]. Microvascular invasion (MVI) is one of the most important factors for recurrence, and a previous study demonstrated that the prevalence of MVI in the specimens obtained from liver resection and transplantation to be between 15 and 57.1% [5], furthermore, in which 69% of patients with MVI have a recurrence of HCC [6]. Thus, accurate preoperative assessment of MVI is of great clinical importance in predicting the prognosis for HCC [7].

Preoperative liver biopsy has been mainly used to prove HCC and detect the histologic grade, but the detection of MVI entails many technical problems such as intratumoral heterogeneity that causes sampling error [8, 9]. Imaging techniques including computed tomography (CT) and magnetic resonance imaging (MRI) can be used to detect MVI based on radiologic features [10]; however, there is still controversy regarding the positive predictive value of radiologic features [11–13]. The use of ^{18}F-fluorodeoxyglucose (^{18}F-FDG) positron emission tomography (PET) to estimate MVI risk has also been proposed and was reported to be useful in patient selection before transplantation [14, 15]. Unfortunately, ^{18}F-FDG PET is not used routinely in HCC imaging because of its limited sensitivity in HCC diagnosis [13, 16]. Diffusion-weighted imaging (DWI) is a noninvasive approach to probe molecular diffusion of water and seems to help predict MVI of HCC [17, 18]. However, the original apparent diffusion coefficient (ADC) is calculated by using the mono-exponential model which ignored the effect of perfusion fraction in tissue and has the limitation to reflect true water diffusion [19, 20].

Multi-*b*-value DW imaging processed with intravoxel incoherent motion (IVIM) can evaluate the true molecular diffusion and perfusion from the blood microcirculation in the capillary networks by using a bi-exponential model calculated with multi-*b*-values and without contrast agent administration. In theory, compared with ADC, IVIM has the ability to analyze non-Gaussian diffusion and thus has the potential to better characterize heterogeneity of tumor components [21, 22]. Furthermore, the abnormal angiogenesis of tumor is also closely related to the heterogeneity of tumor tissue, and the tumor angiogenesis can also directly lead to the occurrence of MVI [23]. More recently, several studies have demonstrated that IVIM-derived parameters showed better diagnostic performance in characterizing and grading rectal cancer, breast cancer, gliomas, and gastric cancer in comparison with ADC [24–27]. Woo et al [28] reported that IVIM model showed significantly better diagnostic performance than ADC in differentiating high-grade HCC from low-grade HCC. In addition, superior performance of IVIM model over ADC was found in the assessment of post therapeutic efficacy in HCC [29, 30]. To our knowledge, few studies [31] have investigated the association between IVIM-derived parameters and the presence of MVI of HCC. The purpose of this study was to prospectively determine the efficacy of IVIM and conventional radiologic features for preoperative prediction of MVI in HCC.

Materials and methods

Participants

This study was approved by the institutional review board, and written informed consent was obtained from all patients. This study was conducted in accordance with the Declaration of Helsinki. Between March 2016 and December 2017, a total of 213 consecutive patients who were suspected of having malignant hepatic lesions identified with ultrasonography or computed tomography (CT) underwent preoperative routine MR and IVIM sequence examination in our institution. Among them, 98 patients were excluded because of the exclusion criteria (Fig. 1). The exclusion criteria were as follows: (a) patients underwent hepatectomy with preoperative transarterial chemoembolization ($n = 21$) or radiofrequency ablation ($n = 17$); (b) hepatectomy cannot be performed because of the diagnosis at late stage ($n = 15$); (c) hepatic lesions were pathologically diagnosed as benign lesions ($n = 13$), intrahepatic cholangiocarcinoma ($n = 13$), or combined HCC ($n = 8$); (d) hepatectomy over 2 weeks after the MR examination ($n = 3$); (e) small HCC lesions in diameter less than 1 cm ($n = 4$); (f) no satisfied MR images were available because of the severe motion and respiratory artifacts ($n = 4$). Finally, 115 patients were remained in this study.

MR imaging

For all examinations, studies were carried out by using a 3.0-T MR system (Discovery MR 750, GE Healthcare). An eight-

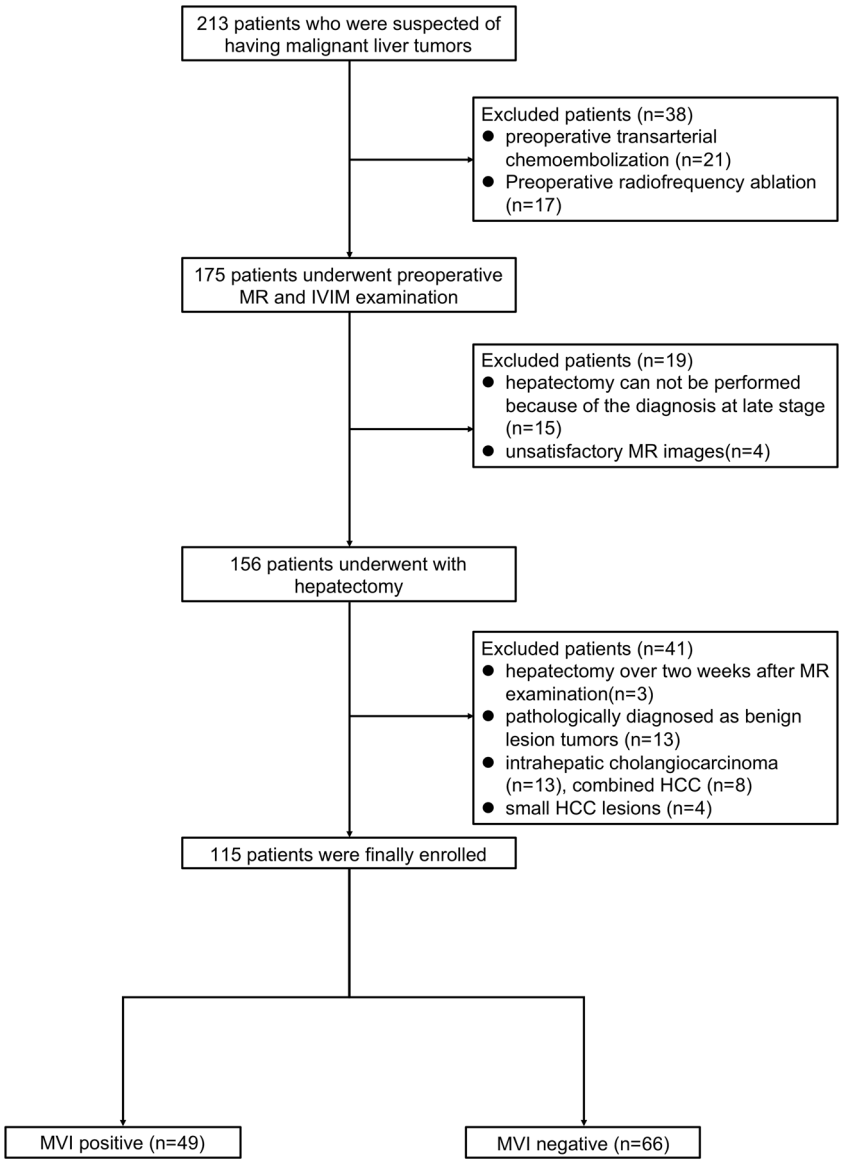

Fig. 1 Flow diagram of the study population. IVIM, intravoxel incoherent motion; MVI, microvascular invasion

channel phased-array torsor coil (GE Medical System) was used for all measurements. Multi-*b*-value DW imaging was performed by using an echo-planner imaging sequence with respiratory gating; the parallel imaging was used to shorten the scanning time and reduce image distortion. The multi-*b*-value DW imaging was performed before the injection of contrast agents. Thirteen *b*-values from 0 to 1200 s/mm^2 (0, 10, 20, 40, 80, 100, 150, 200, 400, 600, 800, 1000, and 1200 s/mm^2) were obtained, and the number of excitations (NEX) for each *b*-value was 1, 6, 4, 2, 2, 2, 1, 1, 2, 4, 6, 6, and 8, respectively. The routine MR imaging sequences included in the standardized scanning protocol were respiratory-triggered axial T2-weighted fast recovery fast spin echo sequence, in and out of phase T1-weighted imaging acquired with fast spoiled gradient-recalled dual-echo sequence, and pre- and postcontrast liver acceleration volume acquisition (LAVA) acquired with gradient recalled echo sequence at arterial phase (20 s), portal venous phase (60 s), and delayed phase (180 s). The detailed parameters of each acquisition sequence are shown in Table 1.

Imaging analysis

All the multi-*b*-value DW images were obtained and transferred to the workstation (Advantage workstation 4.6; GE Medical System). The ADC value was calculated from all 13 *b*-values by using a mono-exponential model with the equation:

$$\frac{S(b)}{S(0)} = \exp(-b \times \mathrm{ADC})$$

Table 1 Parameters of multi-*b*-value DW imaging, T1-weighted imaging, T2-weighted imaging, and LAVA sequence

Parameter	Multi-*b*-value DWI	In/out of phase T1-weighted imaging	T2-weighted imaging	LAVA
Repetition time (ms)	9230	150	6667	4.3
Echo time (ms)	84.7	2.4/5.8	82.6	1.7
Field of view (cm^2)	40 × 30	40 × 40	40 × 40	40 × 32
Scan matrix	80 × 128	288 × 192	320 × 320	260 × 180
Slice thickness (mm)	6	6.5	6.5	4
Slice gap (mm)	2	2	2	2
Number of excitation	…	1	2	1

where $S(b)$ is the signal intensity in the pixel with diffusion gradient b and $S(0)$ is the signal intensity in the pixel without diffusion gradient. Least squares minimization was performed with the Levenberg-Marquardt algorithm for the IVIM fitting of signal data to derive true diffusion coefficient (D), pseudodiffusion coefficient (D^*), and pseudodiffusion component fraction (f), using the below equation:

$$\frac{S(b)}{S(0)} = f\exp\left(-b \times D^*\right) + (1-f)\exp(-b \times D)$$

All the multi-*b*-value DW images were analyzed by two independent radiologists (H.T., Y.W., with 12 and 6 years of experience in reading MR images, respectively) who were blinded to the histopathological results and laboratory tests. For every patient, the whole tumor volume was selected for the region of interest (ROI) measurement (Fig. 2). Each radiologist drew freehand ROI to outline the tumor around the tumor margin on the original DW images ($b = 400$ s/mm^2) on each tumor slice, and try to avoid the hemorrhage, calcified, and necrotic areas; in addition, all the slices where tumor appears were included. The ADC, D, f, and D^* values were automatically calculated by the workstation, and the averaged value of all tumor slice of each parameter was used for further statistical analysis.

Radiologic features evaluation

All MR images were reviewed in our institutional picture archiving and communication system (Syngo-Imaging, version VB36A; Siemens Medical Solutions). The radiologic features were evaluated by two experienced radiologists (B.S., Z.H., with 25 and 8 years of experience in reading MR images, respectively), who were aware that patients had HCC but blinded to the IVIM and clinical outcomes that concern MVI status. The conventional T1- and T2-weighted images and dynamic contrast-enhanced MR images were reviewed; when the two radiologists did not fully agree on the radiologic features, a consensus was achieved by discussion.

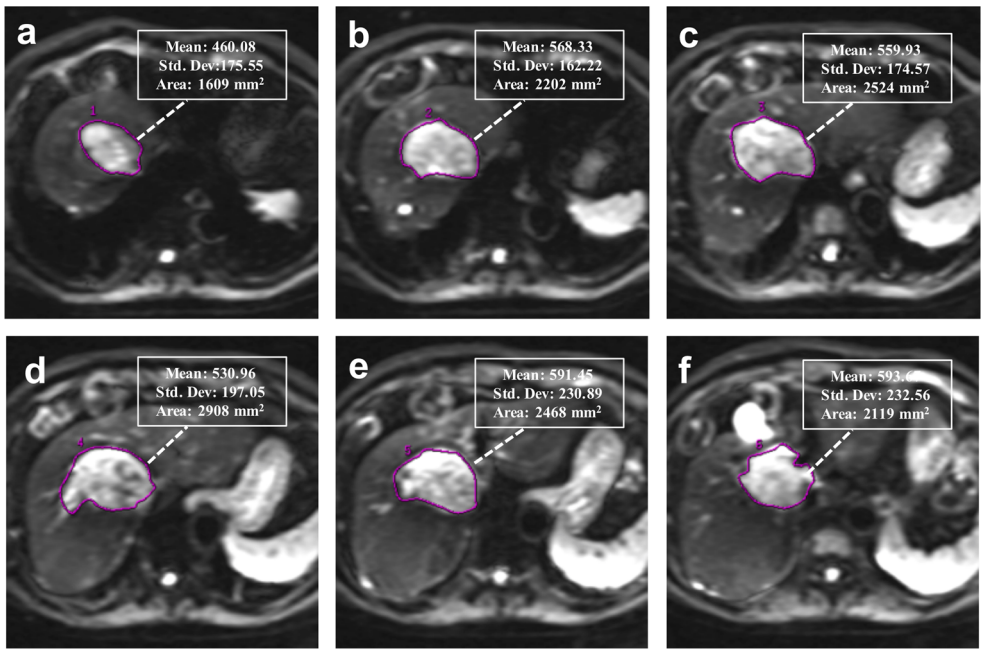

Fig. 2 Regions of interests positioning in a 48-year-old man, the whole tumor slices (**a**-**f**) were selected for the measurement

The two radiologists qualitatively determined the following radiologic features: (a) tumor size: the maximum diameter on the transverse section shown on the portal venous phase or equilibrium phase; (b) number of lesions; (c) tumor margin: which was defined on the portal venous phase or equilibrium phase, and grouped into four categories: smooth margin (smooth nodular tumors in all constructed imaging planes), nonsmooth margin (nonsmooth nodular tumors with focal extranodular growth), nonsmooth margin with multinodular type, and nonsmooth margin with infiltrative border; (d) enhancement pattern: which was defined as typical (arterial phase washin and portal venous or equilibrium phase washout) or atypical enhancement pattern (hypovascular lesion, and lesions only showed washin or washout); (e) tumor capsule: the tumor capsule was defined in the equilibrium phase images identified as a thin, linear and enhanced structure surrounded the tumor and grouped into absence, incomplete, and complete types; (f) peritumoral enhancement: the presence or absence of the peritumoral enhancement was defined as tissue adjacent to the tumor border with arterial phase enhancement and became isointense on the portal venous or equilibrium phase, presence of the peritumoral enhancement was also grouped into wedge-shaped enhancement and irregular circumferential enhancement.

Histopathological examinations

The surgically resected hepatic specimens were used for the pathological evaluation. Identification of the pathological characteristics was performed by a team of experienced pathologists (each individual with more than 10 years of experience in reading histopathological slices), who were blinded to the MR and clinical results. MVI was defined as a tumor within a vascular space lined by endothelium, which was visible only at microscopy. The MVI of tumor cells invasion into the portal branches and capillaries was pathologically examined by using the specimen samples. In addition, the degree of tumor differentiation according to the Edmondson-Steiner grade and the degree of liver fibrosis according to the Metavir fibrosis scoring systems were also recorded [32].

Statistical analysis

Categorical variables are reported as the number of cases and percentages and χ^2 or Fisher's exact test was used for the categorical variables. For the multiple comparison of radiologic features, the α' is adjusted according to the formula $\alpha' = \frac{\alpha}{k-1}$ (k: number of comparisons). Continuous variables were firstly checked for homogeneity by using F test, and independent sample t test or t' test was used for the continuous variables. Interobserver agreement toward the diffusion parameters and radiologic features were checked by using the intra-class correlation coefficient (ICC) with the two-way random method (values < 0.50 poor agreement, 0.51–0.75 moderate agreement, 0.76–0.90 good agreement, > 0.91 excellent agreement) and kappa test (values < 0.40 poor agreement, 0.41–0.60 moderate agreement, 0.61–0.80 substantial agreement, > 0.81 almost excellent agreement). All the data of the IVIM parameters measured by two radiologists were averaged and transformed into a z score normalization to avoid the bias of individual's dimension and used for further univariate and multivariate analyses. Univariate and multivariate logistic regression analyses were used to screen the independent risk factors of MVI, univariate analyze was firstly performed, and only those parameters found to have statistical significance were used for further stepwise multivariate logistic regression. Pearson's chi-square test was used for examining the goodness-of-fit of the multivariate logistic model, and a p value over 0.1 indicates that the model was acceptable. Odds ratio (OR) and 95% confidence interval (CI) were calculated. Receiver operating characteristics (ROC) curves were drawn to assess the area under curve (AUC) of the continuous variables that were statistically significant in the logistic regression. The cutoff point was selected by using the maximized values of Youden indexes, and sensitivity and specificity at the threshold value were determined. A p value less than 0.05 was considered to indicate a statistical significance. All statistical analyses were performed by using a statistical software package (SPSS 23.0 (SPSS Inc.)).

Results

Clinicopathologic characteristics

During the study period, 213 consecutive patients were potentially included. Of these, 115 patients (mean age, 51.97 ± 10.90 years; range, 25–74 years) with 135 HCCs, including 78 (67.8%) men (52.03 ± 11.29 years; range, 29–74 years) and 37 (32.2%) women (51.86 ± 10.19 years; range, 25–65 years), who met the inclusion criteria were included. In the study cohort, 10 patients had multiple HCCs with MVI, and 8 patients had multiple HCCs without MVI (Table 2), 2 patients had three HCCs, and remaining 16 patients had two HCCs. No significant differences of the baseline characteristics were obtained between the MVI-positive and MVI-negative groups (all $p < 0.05$), and baseline characteristics of all patients are summarized in Table 2.

Radiologic features

Of all the 135 HCCs, MVI was present with 55 (40.7%) HCCs and absent with 80 (59.3%) HCCs. As reported in Table 3, only the irregular circumferential enhancement ($p < 0.001$) showed a statistical significance between the MVI-positive

Table 2 Baseline characteristics and histologic findings of the study population

Variable	MVI-positive ($n = 49$)	MVI-negative ($n = 66$)	p value
Age, mean (SD), years*	52.41 ± 10.44	51.65 ± 11.30	0.714
Sex	…	…	0.757
Male	34 (69.4)	44 (66.7)	…
Female	15 (30.6)	22 (33.3)	…
Multi-HCC patients	10 (20.4)	8 (12.1)	0.226
Hepatitis virus infection†	…	…	0.550
Hepatitis B virus	26 (53.1)	37 (56.1)	…
Hepatitis C virus	1 (2.0)	4 (6.1)	…
None	22 (44.9)	25 (37.9)	…
Alanine aminotransferase level, > 50 (IU/l)	9 (18.4)	7 (10.6)	0.234
Aspartate aminotransferase, > 40 (IU/l)	18 (36.7)	20 (30.3)	0.468
Total bilirubin, > 21 (μmol/l)	13 (26.5)	14 (21.2)	0.506
Direct bilirubin, > 7 (μmol/l)	15 (30.6)	18 (27.3)	0.695
γ-Glutamyltransferase, > 60 (IU/l)	20 (40.8)	24 (36.4)	0.627
Alpha fetoprotein > 8 (ng/ml)	17 (34.7)	20 (30.3)	0.618
Carcinoembryonic antigen, > 6.5 (ng/ml)†	3 (6.1)	5 (7.6)	1.000
Cancer antigen 19–9, > 22 (U/ml)	15 (30.6)	17 (25.8)	0.566
Child-Pugh class	…	…	0.748
Child-Pugh A	44 (89.8)	58 (87.9)	…
Child-Pugh B	5 (10.2)	8 (12.1)	…
Edmondson-Steiner grade	…	…	0.669
G1–G2	27 (55.1)	39 (59.1)	…
G3–G4	22 (44.9)	27 (40.9)	…
Fibrosis stage	…	…	0.233
S1–S2	12 (24.5)	23 (34.8)	…
S3–S4	37 (75.5)	43 (65.2)	…

Data are numbers of patients, with percentages in parentheses. *Data are means ± deviation. † Data are compared by using Fisher's exact test. The age is compared by using independent sample t test. Excepted where indicated, data are compared by using χ^2 test

and MVI-negative groups, and the categories of tumor capsule ($p = 0.492$) and tumor margin ($p = 0.487$) showed no significant difference between these two groups. The agreement of radiologic features between the two readers was almost excellent for typical enhancement ($K = 0.89$), peritumoral enhancement ($K = 0.84$), smooth tumor margin ($K = 0.82$), and substantial agreement for presence of tumor capsule ($K = 0.717$).

Diffusion parameters

The ADC value measured by both two radiologists was significantly higher in the MVI-negative group (R1: 1.37 ± 0.37, 10^{-3} mm^2/s; R2: 1.37 ± 0.36, 10^{-3} mm^2/s) than in the MVI-positive group (R1: 1.07 ± 0.27, 10^{-3} mm^2/s; R2: 1.07 ± 0.28, 10^{-3} mm^2/s) (all $p < 0.001$). In addition, the D value was also significantly higher in the MVI-negative group (R1: 1.07 ± 0.34, 10^{-3} mm^2/s; R2: 1.04 ± 0.29, 10^{-3} mm^2/s) compared with the MVI-positive group (R1: 0.77 ± 0.16, 10^{-3} mm^2/s; R2: 0.76 ± 0.16, 10^{-3} mm^2/s) (all $p < 0.001$) (Fig. 3). No statistical significance was observed for D* (R1: $p = 0.103$; R2: $p = 0.093$) and f (R1: $p = 0.745$; R2: $p = 0.724$) in those patients with MVI-positive (Fig. 4) compared with MVI-negative (Fig. 5). The agreements between the two radiologists were excellent for ADC (ICC, 0.957; 95% confidence interval [CI], 0.940–0.969), D (ICC, 0.941; 95% CI, 0.917–0.958), D* (ICC, 0.947; 95% CI, 0.926–0.962), and f (ICC, 0.949 95% CI, 0.929–0.963). The ADC and IVIM parameters measured by two radiologists are listed in Table 4.

Univariate and multivariate analyses

At univariate analysis, the ADC (odds ratio, 0.341; 95% CI, 0.211–0.552; $p < 0.001$), D (odds ratio, 0.141; 95% CI, 0.067–0.299; $p < 0.001$), and irregular circumferential enhancement (odds ratio, 9.908; 95% CI, 3.776–25.996; $p < 0.001$) were found to be statistically significant with the status of MVI. However, no statistical differences were obtained from the baseline characteristics (all $p > 0.05$) nor radiologic features including incomplete tumor capsule ($p = 0.357$), wedge-shaped enhancement ($p = 0.061$), and infiltrative border ($p = 0.254$).

Table 3 Radiologic features and relationship with MVI of 135 HCCs

Radiologic features	Total HCCs ($n = 135$)	MVI-positive ($n = 55$)	MVI-negative ($n = 80$)	p value
Tumor size	…	7.04 ± 3.67 cm	5.80 ± 3.95 cm	0.066
Enhancement pattern	…	…	…	0.716
Typical	98 (72.6)	39 (70.9)	59 (73.8)	…
Atypical	37 (27.4)	16 (29.1)	21 (26.3)	…
Tumor capsule	…	…	…	0.492
Absence	23 (17.0)	11 (20.0)	12 (15.0)	…
Complete	72 (53.3)	26 (47.3)	46 (57.5)	…
Incomplete	40 (29.6)	18 (32.7)	22 (27.5)	…
Peritumoral enhancement	…	…	…	< 0.001
Absence*	51 (37.8)	10 (18.2)	41 (51.3)	…
Wedge-shaped	43 (31.9)	16 (29.1)	27 (33.8)	0.057
Irregular circumferential	41 (30.4)	29 (52.7)	12 (15.0)	< 0.001
Tumor margin	…	…	…	0.487
Smooth	55 (40.7)	19 (34.5)	36 (45)	…
Focal	29 (21.5)	11 (20)	18 (22.5)	…
Multi	26 (19.3)	13 (23.6)	13 (16.3)	…
Infiltrative	25 (18.5)	12 (21.8)	13 (16.3)	…

Data are numbers of lesions, with percentages in parentheses. *Data are used as the reference variable. The tumor size is compared by using independent sample t test. Excepted where indicated, data are compared by using χ^2 test

At multivariate analysis, only D (odds ratio, 0.096; 95% CI, 0.025–0.364; $p = 0.001$) was the independent risk factor for the status of MVI and the ADC ($p = 0.493$) and irregular circumferential enhancement ($p = 0.632$) showed no statistical significance. The Pearson chi-square test showed a value of 117.68 ($p = 0.77$), indicating an acceptable goodness-of-fit of the multivariate model. The ROC curve analysis of the D showed an area under curve (AUC) of 0.815 (95% CI, 0.740–0.877) with the optimal cutoff value of 0.868×10^{-3} mm^2/s; the sensitivity, specificity, and accuracy of D value in the prediction of MVI were 78.2% (43/55), 75.0% (60/80), and 76.3% (103/135). ADC showed the AUC value of 0.746 (95% CI, 0.664–0.817) with the optimal cutoff value of 1.19×10^{-3} mm^2/s. The sensitivity, specificity, and accuracy of ADC in the prediction of MVI were 70.9% (39/55), 65.0% (52/80), and 67.4% (91/135) **(**Fig. 6**)**. Table 5 shows the detailed numerical values of risk factors at univariate and multivariate analyses.

Discussion

In the present study, the difference of diffusion parameters and the radiologic features were evaluated between the MVI-positive and MVI-negative groups and all the risk factors were further screened by using univariate and multivariate logistic regression analyses. The results demonstrated that the ADC and D values were significantly decreased with the presence of MVI in HCC at univariate analysis. Furthermore, the multivariate analysis suggested that only the true diffusion D value from IVIM model was the risk factor for MVI and it yields better diagnostic performance in comparison with ADC derived from the mono-exponential model.

Previous studies showed that IVIM model is superior to the mono-exponential model in characterizing liver malignancy [28, 33, 34]. Klauss et al [35] reported that IVIM-derived D had the largest AUC value for differentiation of hypervascular HCC and focal nodular hyperplasia (FNH). In addition, one previous study on IVIM in evaluation of locoregional therapeutic response in HCC by Shirota et al and another study on the monitoring of vascular disrupting therapy both found better performance using IVIM model rather than mono-exponential analysis [29, 36]. Moreover, Woo et al [28] reported that IVIM-derived D showed significantly better diagnostic performance than ADC values in differentiating high-grade HCC from low-grade HCC. The findings of our study also demonstrated that D value seems to be a more effective biomarker for MVI of HCC compared with ADC value. The superiority of D compared with ADC in evaluating MVI may be because of that the ADC is a non-specific parameter that contains both tissue cellularity (D) and pseudodiffusion component fraction (f) information. As HCC becomes more poorly differentiated during hepatocarcinogenesis, the cellular density and pseudodiffusion component increase; however, the combined effect of cellular density and pseudodiffusion

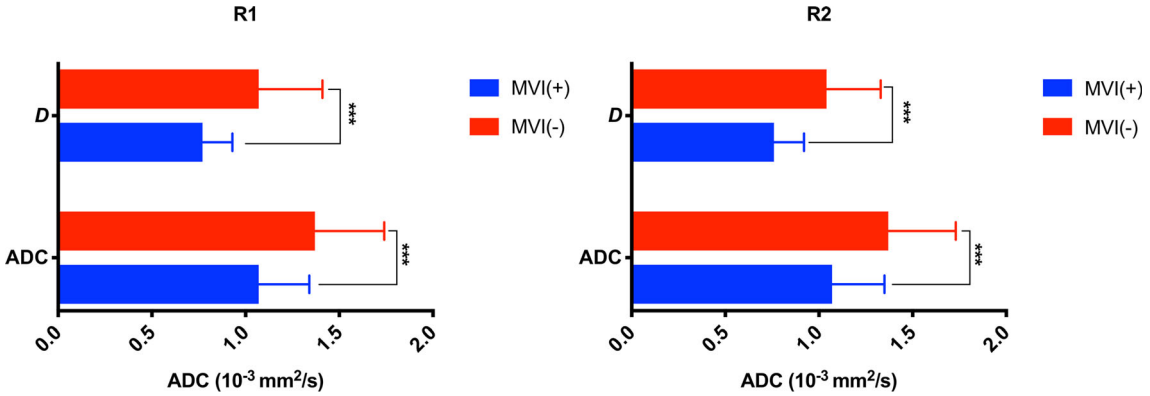

Fig. 3 ADC and *D* values of MVI-positive and MVI-negative groups measured by two radiologists. The ADC and *D* of the MVI-negative group were significantly higher than those of the MVI-positive group (***$p < 0.001$). ADC and *D* were compared by using *t*′ test between the two groups

component will lead to an increase in ADC, whereas the *D* would not be affected [28, 37].

Diffusion parameters, such as the ADC and mean kurtosis, have been demonstrated to be helpful in detecting the MVI of HCC. Previous study showed that ADC was associated with the MVI quantitatively in HCC [18], and another study also showed that mean kurtosis was potential predictive biomarkers for MVI of HCC [37]. The results of our current study showed that ADC and *D* values were significantly higher in MVI-negative than in MVI-positive HCCs. The decreased ADC and *D* values in MVI-positive HCCs may be the presence of tumor emboli or clusters of cancer cells in branches of hepatic vessels such as the portal vein, hepatic vein, and intracapsular vessel which could restrict the diffusion of water molecules [21]. In addition, the presence of MVI may further increase the infiltration of tumor cells and provide more nutrition for the proliferation and make the tumor more densely cell-packed structures, which may further restrict the diffusion of water molecular and decrease the ADC and *D* values. Furthermore, the decreased ADC value was statistically significant in HCCs with MVI by using univariate analysis, but the results of multivariate analysis did not indicate that ADC was an independent risk factor for MVI of HCC. This might be explained by the fact that the pseudodiffusion component can affect the ADC measurement; however, the true diffusion coefficient (*D*) would not be affected.

Our data demonstrated that the perfusion parameters *D** and *f* were not statistically significant in predicting the MVI of HCC. In theory, *D** is correlated with the average blood flow rate and *f* could reflect the fraction volume of capillary blood flow, both of which could be used to reflect the vascularity in tissue [28, 29]. However, *D** and *f* values in MVI-positive and MVI-negative showed no statistical significance in our study. The current result may be attributed to the overlap of the blood supply during the poorly differentiated process, which may obscure the sensitivity of *D** and *f* [38]. The result of our preliminary study was consistent with that of the previous study in predicting the histologic grade of HCC by using IVIM which demonstrated that *D** and *f* were not statistically different among HCC Edmondson-Steiner grades.

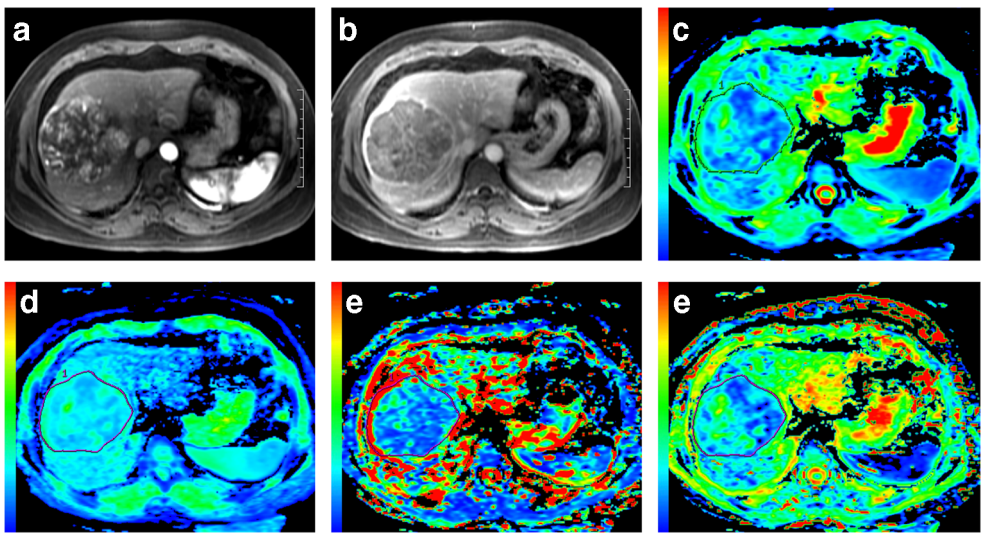

Fig. 4 Surgically confirmed HCC with MVI in a 54-year-old man. (**a**) Arterial phase image shows a lobulated mass with heterogeneous enhancement followed by washout seen in (**b**) portal venous phase. (**c**) ADC map, ADC value for the lesion was 1.12×10^{-3} mm^2/s. (**d**) *D* map, *D* value for the lesion was 0.80×10^{-3} mm^2/s. (**e**) *D** map, *D** value for the lesion was 9.55×10^{-3} mm^2/s. (**f**) *f* map, *f* value was 0.237 × 100%. ADC and *D* maps show a slightly higher signal intensity compared with that of liver parenchyma

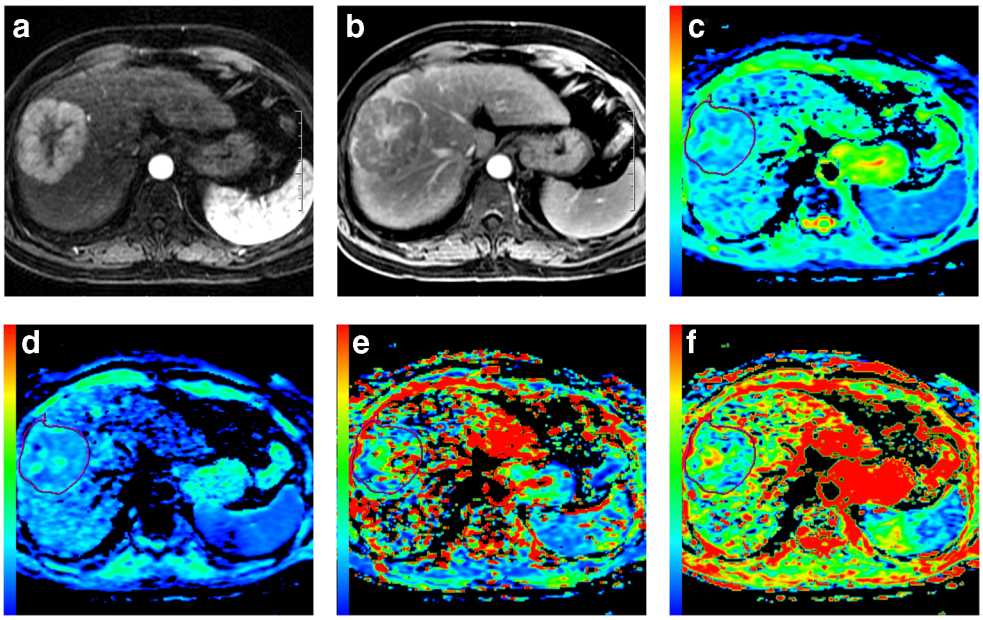

Fig. 5 Surgically confirmed HCC without MVI in a 58-year-old woman. **a** Arterial phase image shows a round mass with heterogeneous enhancement followed by washout seen in (**b**) portal venous phase. **c** ADC map, ADC value for the lesion was 1.38×10^{-3} mm^2/s. **d** *D* map, *D* value for the lesion was 1.18×10^{-3} mm^2/s. **e** *D** map, *D** value for the lesion was 15.8×10^{-3} mm^2/s. **f** *f* map, (*f*) value was 0.308 × 100%. ADC and *D* maps show a slightly higher signal intensity compared with that of liver parenchyma

Furthermore, the respiratory artifact, relaxation effects, and T2 contribution may also influence the accuracy of perfusion parameter [39].

Our data demonstrated that some "worrisome" radiologic features [12] including the incomplete tumor capsule, infiltrative border, and irregular circumferential peritumoral enhancement were not confirmed as reliable predictors for MVI. Histologically, the fibrous capsule consists of an inner layer rich in pure, fibrous tissue and an outer layer containing portal venules (or sinusoids) and newly formed bile ducts [40], which can act as a barrier to inhibit HCC dissemination. Once the tumor cells invade into and break through the portal venules of the capsule, imaging signs of the incomplete capsule and infiltrative border appear. Furthermore, the peritumoral enhancement may be related with hemodynamic perfusion changes existing in compensatory arterial hyperperfusion, which can often occur in the area of decreased portal flow as the minute portal venule occlusion caused by tumor thrombi [12, 38]. Previous study by Wang et al [37] showed that the irregular circumferential enhancement was significantly correlated with MVI, and another study conducted by Matteo et al [13] reported that both nonsmooth tumor margin and peritumoral enhancement were significant in predicting MVI. However, Chou et al [41] found that only nonsmooth tumor margin correlated with the presence of MVI. These results of the different studies were inconsistent in varying degrees. Three possible reasons might be used to explain the discrepancies in these findings. First, the different study designs, as the prospective and retrospective study designs coexisted in these findings, and the selection bias of patients might influence the results. Second, the difference of imaging resolutions between CT and MR and higher soft tissue resolution of MR entail a more clear depiction of the details around the tumor, which may achieve a high diagnostic accuracy of MVI. Third, the difference between different contrast agent concentrations may also influence the depiction of the peritumoral enhancement of small vessels, as high concentration of the contrast agent is more feasible in displaying small vessels.

We acknowledge some limitations of our study. First, the limited number of MVI-positive samples leaves the question open on the statistical power; therefore, we should continue to

Table 4 ADC and IVIM parameters between the MVI-negative and MVI-positive groups and the agreements between two radiologists

Parameters	Radiologist 1			Radiologist 2			ICC
	MVI-negative	MVI-positive	*p* value	MVI-negative	MVI-positive	*p* value	
ADC	1.37 ± 0.37	1.07 ± 0.27	< 0.001	1.37 ± 0.36	1.07 ± 0.28	< 0.001	0.957
D	1.07 ± 0.34	0.77 ± 0.16	< 0.001	1.04 ± 0.29	0.76 ± 0.16	< 0.001	0.941
*D**	17.88 ± 12.68	14.38 ± 11.40	0.103	17.39 ± 11.41	13.99 ± 11.62	0.093	0.947
f	0.36 ± 0.14	0.36 ± 0.16	0.745	0.36 ± 0.14	0.37 ± 0.16	0.724	0.949

ADC, *D*, and *D** are in units of 10^{-3} mm^2/s, *f* is in the unit of 100%. The ADC and *D* were compared by using *t'* test, *D** and *f* were compared by using *t* test

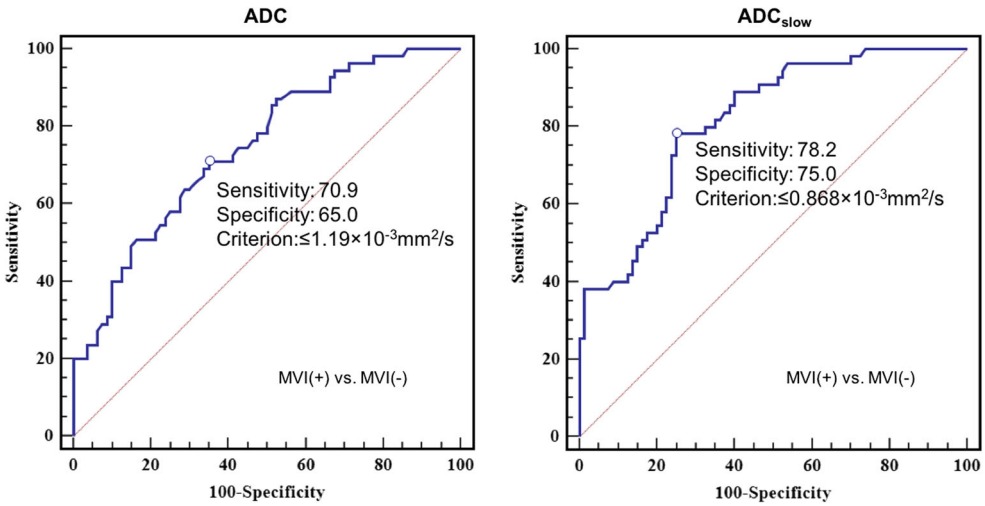

Fig. 6 ROC curves of ADC and *D* to distinguish MVI-positive and MVI-negative HCCs. AUC value of ADC was 0.746 (95% CI, 0.664–0.817) with the optimal cutoff value of 1.19×10^{-3} mm^2/s, AUC value of *D** was 0.815 (95% CI, 0.740–0.877) with the optimal cutoff value of 0.868×10^{-3} mm^2/s

Table 5 Univariate and multivariate analyses of the risk factors of MVI status

Risk factors	Univariate analysis			Multivariate analysis		
	Odds ratio	95% CI	*p*	Odds ratio	95% CI	*p*
Age, mean (SD), years	1.006	0.973–1.041	0.712	…	…	…
Tumor size	1.088	0.994–1.191	0.068	…	…	…
Multi-HCCs	1.859	0.674–5.127	0.231	…	…	…
Hepatitis B infection	0.886	0.422–1.861	0.749	…	…	…
Alpha fetoprotein > 8 (ng/ml)	1.222	0.555–2.688	0.618	…	…	…
Carcinoembryonic antigen, > 6.5 (ng/ml)	0.796	0.181–3.501	0.762	…	…	…
Cancer antigen 19-9, > 22 (U/ml)	1.272	0.560–2.889	0.566	…	…	…
Child-Pugh class	0.824	0.252–2.692	0.748	…	…	…
Edmondson-Steiner grade	1.177	0. 558–2.484	0.669	…	…	…
Fibrosis stage	1.649	0.723–3.763	0.234	…	…	…
Atypical enhancement	1.153	0.536–2.479	0.716	…	…	…
Tumor capsule incomplete	1.448	0.659–3.180	0.357	…	…	…
Tumor capsule absence	1.622	0.628–4.189	0.318			
Peritumoral enhancement	…	…	…	…	…	…
Absence*	…	…	…	…	…	…
Wedge-shaped	2.430	0.961–6.142	0.061	…	…	…
Irregular circumferential	9.908	3.776–25.996	< 0.001†	0.759	0.245–2.351	0.632
Tumor margin	…	…	…	…	…	…
Smooth*	…	…	…	…	…	…
Focal	1.158	0.455–2.945	0.758	…	…	…
Multi	1.895	0.734–4.892	0.187	…	…	…
Infiltrative	1.749	0.669–4.575	0.254	…	…	…
ADC^{Π}	0.341	0.211–0.552	< 0.001†	1.330	0.589–3.002	0.493
D^{Π}	0.141	0.067–0.299	< 0.001†	0.096	0.025–0.364	0.001‡
$D^{*\Pi}$	0.731	0.505–1.058	0.097	…	…	…
f^{Π}	1.063	0.754–1.498	0.729	…	…	…

*Data were used as the reference variable. † Data are statistically from the univariate logistic regression. ‡ Data are statistically from the multivariate logistic regression. $^{\Pi}$ Data at univariate and multivariate logistic analyses were transformed into a *z* normalization

collect more samples. Second, this is a single-center study with a single MR unit; it is necessary to validate the results from other centers. Third, HCC was only assessed by either absence or presence of MVI, but critical matching between the histopathological slice and DW image is difficult to achieve. Thus, in our study, whole tumor volume was measured to overcome this limitation and we found that the trend of decreased *D* value was useful in predicting MVI of HCC. Finally, in this study, the acquisition time was relatively long as multi-*b*-values were obtained for IVIM model calculation. One previous study conducted by Muertz et al [42] found that IVIM model can be achieved with only three-*b*-value DWI and the parameters of *D* and *f* provided more discriminatory power between liver lesions than ADC. Therefore, the simplified IVIM should be further investigated as which could greatly short acquisition time.

In conclusion, IVIM model–derived *D* value is superior to ADC measured with mono-exponential model for evaluating the MVI of HCC, and the multi-*b*-value DWI acquisition is also recommended even with longer acquisition time, which entails the IVIM model calculation. Among MR imaging features, tumor margin, enhancement pattern, tumor capsule, and peritumoral enhancement were not predictive for MVI. We believe that preoperative identification of patients at high risk for MVI will help improve overall care for patients undergoing hepatectomy.

Funding This study was funded by Research Grant of National Nature Science Foundation of China and Science (Grant number 81471658) and Technology Support Program of Sichuan Province (Grant number 2017SZ0003) and Science and Technology Support Program of Sichuan Province (Grant number 2017SZ0185).

Compliance with ethical standards

Guarantor The scientific guarantor of this publication is Bin Song.

Conflict of interest The authors of this manuscript declare no relationships with any companies, whose products or services may be related to the subject matter of the article.

Statistics and biometry One of the authors (Yi Wei) has significant statistical expertise.

Informed consent Written informed consent was obtained from all subjects (patients) in this study.

Ethical approval Institutional Review Board approval was obtained.

Methodology
- prospective
- diagnostic study
- performed at one institution

References

1. Torre LA, Bray F, Siegel RL, Ferlay J, Lortet-Tieulent J, Jemal A (2015) Global cancer statistics, 2012. CA Cancer J Clin 65:87–108
2. Kudo M, Trevisani F, Abou-Alfa GK, Rimassa L (2016) Hepatocellular carcinoma: therapeutic guidelines and medical treatment. Liver Cancer 6:16–26
3. Forner A, Llovet JM, Bruix J (2012) Hepatocellular carcinoma. Lancet 379:1245–1255
4. Hirokawa F, Hayashi M, Asakuma M, Shimizu T, Inoue Y, Uchiyama K (2016) Risk factors and patterns of early recurrence after curative hepatectomy for hepatocellular carcinoma. Surg Oncol 25:24–29
5. Rodriguez-Peralvarez M, Luong TV, Andreana L, Meyer T, Dhillon AP, Burroughs AK (2013) A systematic review of microvascular invasion in hepatocellular carcinoma: diagnostic and prognostic variability. Ann Surg Oncol 20:325–339
6. Witjes CD, Willemssen FE, Verheij J et al (2012) Histological differentiation grade and microvascular invasion of hepatocellular carcinoma predicted by dynamic contrast-enhanced MRI. J Magn Reson Imaging 36:641–647
7. An C, Kim MJ (2018) Imaging features related with prognosis of hepatocellular carcinoma. https://doi.org/10.1007/s00261-018-1758-y
8. Pawlik TM, Gleisner AL, Anders RA, Assumpcao L, Maley W, Choti MA (2007) Preoperative assessment of hepatocellular carcinoma tumor grade using needle biopsy: implications for transplant eligibility. Ann Surg 245:435–442
9. Ramos Rubio E, Llado Garriga L (2010) [Usefulness of pre-surgical biopsy in selecting patients with hepatocellular carcinoma for liver transplant]. Cir Esp 87:133–138
10. Unal E, Idilman IS, Akata D, Ozmen MN, Karcaaltincaba M (2016) Microvascular invasion in hepatocellular carcinoma. Diagn Interv Radiol 22:125–132
11. Hirokawa F, Hayashi M, Miyamoto Y et al (2014) Outcomes and predictors of microvascular invasion of solitary hepatocellular carcinoma. Hepatol Res 44:846–853
12. Renzulli M, Brocchi S, Cucchetti A et al (2016) Can current preoperative imaging be used to detect microvascular invasion of hepatocellular carcinoma? Radiology 279:432–442
13. Jiang HY, Chen J, Xia CC, Cao LK, Duan T, Song B (2018) Noninvasive imaging of hepatocellular carcinoma: from diagnosis to prognosis. World J Gastroenterol 24:2348–2362
14. Lim C, Salloum C, Chalaye J et al (2018) 18F-FDG PET/CT predicts microvascular invasion and early recurrence after liver resection for hepatocellular carcinoma: a prospective observational study. HPB (Oxford). https://doi.org/10.1016/j.hpb.2018.10.007
15. Yaprak O, Acar S, Ertugrul G, Dayangac M (2018) Role of pretransplant 18F-FDG PET/CT in predicting hepatocellular carcinoma recurrence after liver transplantation. World J Gastrointest Oncol 10:336–343
16. Reginelli A, Vacca G, Segreto T et al (2018) Can microvascular invasion in hepatocellular carcinoma be predicted by diagnostic imaging? A critical review. Future Oncol. https://doi.org/10.2217/fon-2018-0175
17. Wei Y, Gao F, Wang M et al (2019) Intravoxel incoherent motion diffusion-weighted imaging for assessment of histologic grade of hepatocellular carcinoma: comparison of three methods for positioning region of interest. Eur Radiol 29:535–544
18. Xu P, Zeng M, Liu K, Shan Y, Xu C, Lin J (2014) Microvascular invasion in small hepatocellular carcinoma: is it predictable with

preoperative diffusion-weighted imaging? J Gastroenterol Hepatol 29:330–336
19. Valerio M, Zini C, Fierro D et al (2016) 3T multiparametric MRI of the prostate: does intravoxel incoherent motion diffusion imaging have a role in the detection and stratification of prostate cancer in the peripheral zone? Eur J Radiol 85:790–794
20. Marzi S, Piludu F, Sanguineti G et al (2017) The prediction of the treatment response of cervical nodes using intravoxel incoherent motion diffusion-weighted imaging. Eur J Radiol 92:93–102
21. Iima M, Le Bihan D (2016) Clinical intravoxel incoherent motion and diffusion MR imaging: past, present, and future. Radiology 278(1):13–32
22. Meeus EM, Zarinabad N, Manias KA et al (2018) Diffusion-weighted MRI and intravoxel incoherent motion model for diagnosis of pediatric solid abdominal tumors. J Magn Reson Imaging 47: 1475–1486
23. Yuan SX, Yang F, Yang Y et al (2012) Long noncoding RNA associated with microvascular invasion in hepatocellular carcinoma promotes angiogenesis and serves as a predictor for hepatocellular carcinoma patients' poor recurrence-free survival after hepatectomy. Hepatology 56(6):2231–2241
24. Nougaret S, Vargas HA, Lakhman Y et al (2016) Intravoxel incoherent motion-derived histogram metrics for assessment of response after combined chemotherapy and radiation therapy in rectal cancer: initial experience and comparison between single-section and volumetric analyses. Radiology 280:446–454
25. Suo S, Lin N, Wang H et al (2015) Intravoxel incoherent motion diffusion-weighted MR imaging of breast cancer at 3.0 tesla: comparison of different curve-fitting methods. J Magn Reson Imaging 42:362–370
26. Shen N, Zhao L, Jiang J et al (2016) Intravoxel incoherent motion diffusion-weighted imaging analysis of diffusion and microperfusion in grading gliomas and comparison with arterial spin labeling for evaluation of tumor perfusion. J Magn Reson Imaging 44:620–632
27. Song XL, Kang HK, Jeong GW et al (2016) Intravoxel incoherent motion diffusion-weighted imaging for monitoring chemotherapeutic efficacy in gastric cancer. World J Gastroenterol 22:5520–5531
28. Woo S, Lee JM, Yoon JH, Joo I, Han JK, Choi BI (2014) Intravoxel incoherent motion diffusion-weighted MR imaging of hepatocellular carcinoma: correlation with enhancement degree and histologic grade. Radiology 270:758–767
29. Joo I, Lee JM, Han JK, Choi BI (2014) Intravoxel incoherent motion diffusion-weighted MR imaging for monitoring the therapeutic efficacy of the vascular disrupting agent CKD-516 in rabbit VX2 liver tumors. Radiology 272:417–426
30. Lee Y, Lee SS, Kim N et al (2015) Intravoxel incoherent motion diffusion-weighted MR imaging of the liver: effect of triggering methods on regional variability and measurement repeatability of quantitative parameters. Radiology 274:405–415
31. Li H, Zhang J, Zheng Z et al (2018) Preoperative histogram analysis of intravoxel incoherent motion (IVIM) for predicting microvascular invasion in patients with single hepatocellular carcinoma. Eur J Radiol 105:65–71
32. Amin MB, Edge SB, Greene FL et al (2017) AJCC cancer staging manual, 8th edn. Springer, New York
33. Jerjir N, Bruyneel L, Haspeslagh M, Quenet S, Coenegrachts K (2017) Intravoxel incoherent motion and dynamic contrast-enhanced MRI for differentiation between hepatocellular adenoma and focal nodular hyperplasia. Br J Radiol 90:20170007
34. Choi IY, Lee SS, Sung YS et al (2017) Intravoxel incoherent motion diffusion-weighted imaging for characterizing focal hepatic lesions: correlation with lesion enhancement. J Magn Reson Imaging 45: 1589–1598
35. Klauss M, Mayer P, Maier-Hein K et al (2016) IVIM-diffusion-MRI for the differentiation of solid benign and malign hypervascular liver lesions-evaluation with two different MR scanners. Eur J Radiol 85:1289–1294
36. Shirota N, Saito K, Sugimoto K, Takara K, Moriyasu F, Tokuuye K (2016) Intravoxel incoherent motion MRI as a biomarker of sorafenib treatment for advanced hepatocellular carcinoma: a pilot study. Cancer Imaging 16(1)
37. Wang WT, Yang L, Yang ZX et al (2018) Assessment of microvascular invasion of hepatocellular carcinoma with diffusion kurtosis imaging. Radiology 286:571–580
38. Matsui O, Kobayashi S, Sanada J et al (2011) Hepatocelluar nodules in liver cirrhosis: hemodynamic evaluation (angiography-assisted CT) with special reference to multi-step hepatocarcinogenesis. Abdom Imaging 36:264–272
39. Jerome NP, d'Arcy JA, Feiweier T et al (2016) Extended T2-IVIM model for correction of TE dependence of pseudo-diffusion volume fraction in clinical diffusion-weighted magnetic resonance imaging. Phys Med Biol 61:N667–n680
40. Cho ES, Choi JY (2015) MRI features of hepatocellular carcinoma related to biologic behavior. Korean J Radiol 16:449–464
41. Chou CT, Chen RC, Lin WC, Ko CJ, Chen CB, Chen YL (2014) Prediction of microvascular invasion of hepatocellular carcinoma: preoperative CT and histopathologic correlation. AJR Am J Roentgenol 203:W253–W259
42. Mürtz P, Sprinkart AM, Reick M et al (2018) Accurate IVIM model-based liver lesion characterisation can be achieved with only three b-value DWI. Eur Radiol 28:4418–4428